Transferable Potentials for Phase Equilibria. 1. United-Atom Description of *n*-Alkanes

Marcus G. Martin and J. Ilja Siepmann*

Department of Chemistry, University of Minnesota, 207 Pleasant Street SE, Minneapolis, Minnesota 55455-0431

Received: August 4, 1997; In Final Form: January 23, 1998

A new set of united-atom Lennard-Jones interaction parameters for *n*-alkanes is proposed from fitting to critical temperatures and saturated liquid densities. Configurational-bias Monte Carlo simulations in the Gibbs ensemble were carried out to determine the vapor−liquid coexistence curves for methane to dodecane using three united-atom force fields: OPLS [Jorgensen, et al. *J. Am. Chem. Soc.* **1984**, *106*, 813], SKS [Siepmann, et al. *Nature* **1993**, *365*, 330], and TraPPE. Standard specific densities and the high-pressure equation-of-state for the transferable potentials for phase equilibria (TraPPE) model were studied by simulations in the isobaric−isothermal and canonical ensembles, respectively. It is found that one set of methyl and methylene parameters is sufficient to accurately describe the fluid phases of all *n*-alkanes with two or more carbon atoms. Whereas other *n*-alkane force fields employ methyl groups that are either equal or larger in size than the methylene groups, it is demonstrated here that using a smaller methyl group yields a better fit to the set of experimental data. As should be expected from an effective pair potential, the new parameters do not reproduce experimental second virial coefficients. Saturated vapor pressures and densities show small, but systematic deviation from the experimental data.

1. Introduction

n-Alkanes are nonpolar, flexible chain molecules that are composed of only two types of segments, namely, methyl and methylene groups. *n*-Alkanes are the basic feedstock for all chemical industries and are one of the main building blocks for biological molecules. Therefore, a wealth of experimental thermophysical data exists for the *n*-alkanes, and they are the logical starting point when developing and testing force fields to describe intermolecular interactions. Two different approaches for dividing alkanes into interaction sites are usually followed when building a transferable, molecular force field. The first approach is to treat each hydrogen and carbon atom as an interaction site,[1] and these two types of interaction sites might, in principle, be sufficient to describe all alkanes (methane, linear, and branched). The second approach is to unite each carbon and its bonded hydrogens into a single interaction site,[2] which leads to the introduction of CH_4, CH_3, CH_2, CH, and C pseudoatoms. The former approach is obviously more realistic and is believed to be more appropriate for the solid state and close to the triple point, but the latter reduces the number of interaction sites by a factor of roughly 3 and thus the computational burden by an order of magnitude. A somewhat intermediate alternative would be to use anisotropic (not spherically symmetric) potentials centered at carbon atoms,[3] or to displace the position of the pseudoatom interaction site away from the carbon atom position.[4]

The motivation for this work was to find an optimized set of Lennard-Jones (LJ) methyl and methylene parameters for the normal alkanes using a conventional united-atom description. Molecular simulations for three sets of *n*-alkane parameters (force fields) are described in this paper. Here we should mention also other recent united-atom alkane force fields for which simulations were not performed.[5,6] The popular OPLS (optimized potentials for liquid simulations) united-atom model of Jorgensen et al.[7] was parametrized using isobaric−isothermal Monte Carlo simulations to give accurate liquid densities and heats of vaporization for short alkanes at atmospheric pressure. The OPLS force field contains different LJ parameters for methyl groups in ethane, for methyl groups in all other *n*-alkanes, and for the methylene groups ($\sigma_{CH3}^{ethane} \neq \sigma_{CH_3} = \sigma_{CH_2}$, $\epsilon_{CH3}^{ethane} \neq \epsilon_{CH_3} \neq \epsilon_{CH_2}$, for a total of five LJ parameters). Siepmann, Karaborni, and Smit (SKS) subsequently used configurational-bias Monte Carlo in the Gibbs ensemble to compute the vapor−liquid coexistence curves (VLCC) of *n*-alkanes containing from 5 to 48 carbons.[8−10] They found that the OPLS force field overestimated the critical temperatures of the *n*-alkanes and proposed a new force field (SKS),[9] which gave improved results for medium to long *n*-alkanes. However, the SKS force field overestimates the critical temperatures of the shorter alkanes. The SKS force field uses the same LJ diameter, but different magnitudes of the well depth, to account for methyl and methylene groups ($\sigma_{CH_3} = \sigma_{CH_2}$, $\epsilon_{CH_3} \neq \epsilon_{CH_2}$, for a total of three LJ parameters). The third molecular model used is the new transferable potentials for phase equilibria (TraPPE) force field. As for the SKS force field, the TraPPE force field is based on calculations of VLCC. For the TraPPe force field, however, the methyl group LJ parameters were obtained first from simulations of ethane and then retained for the longer alkanes. The methylene group parameters were fitted to the VLCC of *n*-octane. This strategy results in different sizes and well depths of the methyl and methylene beads ($\sigma_{CH_3} \neq \sigma_{CH_2}$, $\epsilon_{CH_3} \neq \epsilon_{CH_2}$, for a total of four LJ parameters).

The OPLS, SKS, and TraPPE force fields are built around the following set of constraints: one common C−C bond length, one common C−C−C bond angle and bending force constant, and one common dihedral potential. These force fields are all subsets of a 10-parameter united-atom *n*-alkane model that would have five different pseudoatoms (two methyl pseudo-

* Corresponding author: siepmann@chem.umn.edu.

S1089-5647(97)02543-1 CCC: $15.00
Published on Web 03/17/1998

TABLE 1: Comparison of the Lennard-Jones Parameters for the OPLS,[7] SKS,[9,10] and TraPPE Force Fields

	OPLS		SKS		TraPPE	
pseudoatom	ϵ/k_B [K]	σ [Å]	ϵ/k_B [K]	σ [Å]	ϵ/k_B [K]	σ [Å]
CH_4	147.9	3.73	N/A	N/A	148	3.73
CH_3 (ethane)	104.1	3.775	114	3.93	98	3.75
CH_3 (*n*-alkane)	88.1	3.905	114	3.93	98	3.75
CH_2	59.4	3.905	47	3.93	46	3.95

atoms for $\mathbf{CH_3}-CH_3$ and $\mathbf{CH_3}-CH_2$ and three methylene pseudoatoms for $CH_3-\mathbf{CH_2}-CH_3$, $CH_3-\mathbf{CH_2}-CH_2$, and $CH_2-\mathbf{CH_2}-CH_2$). While it would be possible, but rather tedious, to fit such a model for the linear alkanes, this approach is not feasible for a more general force field because all LJ parameters require to be fitted for all combinations of bonded neighbors. For example, in the case of branched alkanes, a ternary CH pseudoatom has four distinct neighbors, which could be either CH_3, CH_2, CH, or C segments. Thus, more than 10 different CH pseudoatoms would be required. Therefore, we feel that a more general force field has to sacrifice minor gains in accuracy for simplicity at this point, and the TraPPE pseudoatom parameters do not depend upon their neighbors.

This paper is organized as follows. First we briefly describe the three alkane force fields and the simulation methods used. Then we report and discuss single-component data obtained for the three force fields, including VLCC, critical points, boiling points, standard specific densities, high-pressure *PVT* behavior, second virial coefficients, radial distribution functions, and conformational statistics. A report on results for simulation of multicomponent phase equilibria (octane/dodecane boiling point diagram at 20 kPa, (supercritical) ethane/heptane pressure−composition diagram at 366 K, and helium to heptane free energies of transfer for pentane and hexane at standard conditions) using a preliminary version of the TraPPE force field was published elsewhere.[11] The second paper in this series[12] will describe the extension of the TraPPE force field to branched alkanes. Eventually, the TraPPE force field should include a wide range of organic functional groups.

2. Models

The OPLS, SKS, and TraPPE alkane models are based on the united-atom description. In all three cases, the nonbonded interactions between pseudoatoms, which are separated by more than three bonds or belong to different molecules, are described solely by pairwise-additive Lennard-Jones 12−6 potentials,

$$u(r_{ij}) = 4\epsilon_{ij}\left[\left(\frac{\sigma_{ij}}{r_{ij}}\right)^{12} - \left(\frac{\sigma_{ij}}{r_{ij}}\right)^{6}\right] \tag{1}$$

where r_{ij}, ϵ_{ij}, and σ_{ij} are the separation, LJ well depth, and LJ size, respectively, for the pair of atoms i and j. The LJ parameters for interactions between like pseudoatoms (either CH_4, CH_3, or CH_2) are listed in Table 1. Unlike interactions are computed using standard Lorentz−Berthelot combining rules[13,14]

$$\sigma_{ij} = (\sigma_{ii} + \sigma_{jj})/2 \tag{2}$$

$$\epsilon_{ij} = \sqrt{\epsilon_{ii}\epsilon_{jj}} \tag{3}$$

Pseudoatoms are connected by bonds with a fixed length of 1.53 Å for the OPLS model and 1.54 Å for the SKS and TraPPE force fields. In all cases, bond angle bending is governed by a harmonic potential

$$u_{bend} = k_\theta(\theta - \theta_0)^2/2 \tag{4}$$

with the force constant proposed by van der Ploeg and Berendsen;[15] that is, $k_\theta/k_B = 62\,500$ K rad^{-2}, where k_B is Boltzmann's constant. The equilibrium angle θ_0 is set to 112° for OPLS and 114° for SKS and TraPPE. In all cases, the motion of the dihedral angles ϕ is governed by the OPLS united-atom torsional potential,[7]

$$u_{tors} = c_1[1 + \cos\phi] + c_2[1 - \cos(2\phi)] + c_3[1 + \cos(3\phi)] \tag{5}$$

with $c_1/k_B = 355.03$ K, $c_2/k_B = -68.19$ K, and $c_3/k_B = 791.32$ K.

3. Simulation and Analysis Methods

A. Vapor−Liquid Coexistence Curves. A combination[16,17] of the Gibbs ensemble Monte Carlo (GEMC) technique[18−20] and the configurational-bias Monte Carlo (CBMC) method[21−24] was used to determine the VLCC. Since GEMC and CBMC are now well established, only the simulation details specific to this work are discussed. The isometric (*NVT*) version of the Gibbs ensemble utilizes two simulation boxes that have no explicit interface, but are kept in thermodynamic contact by exchanging volume and molecules between the boxes. In the case of flexible chain molecules, three additional types of Monte Carlo moves involving only individual molecules are necessary to sample the remaining degrees of freedom of the combined systems: (i) translation of the center-of-mass (COM), (ii) rotation about the COM,[25] and (iii) configurational-bias regrowth to change the internal conformation. During the course of the Markov chain, the type of move to be attempted is selected with fixed probability from the five available moves. These probabilities were adjusted to yield approximately one accepted volume move (with the maximum volume displacement adjusted to give a 50% acceptance rate) and one accepted molecule exchange move per 10 MC cycles (one cycle consists of N moves, where N is the total number of molecules), with the remainder of the moves equally divided between translation, rotation, and (for molecules with more than two pseudoatoms) CBMC. For the latter three types, the chain to be moved is selected at random. The maximum displacements for translations and rotations are adjusted independently in each box to give a 50% acceptance rate, with an absolute maximum of twice the potential truncation (see below) for translations and π for rotations. The absolute maxima are usually reached in the vapor box at lower temperatures, and therefore the acceptance rates can be higher than 50% in the vapor-phase box. CBMC conformational changes and swaps between boxes are carried out using six to eight trial sites per step in order to sample the gauche and trans states at a reasonable computational expense. Either (i) the positions of the trial sites were selected randomly from a unit sphere followed by a Boltzmann rejection step to account for the bending and torsional potentials,[10,26] or (ii) the bond angle was drawn first from a modified Gaussian distribution, followed by Boltzmann selection of the torsional angle.[27,28] A 5-fold increase in the molecule exchange acceptance rate was realized by performing a biased selection of the first interaction site from 10 random trial positions.[29,30]

The Lennard-Jones interactions were truncated at $r_{cut} = 14$ Å and analytical tail corrections were applied.[31] A hard inner cutoff was also used such that if two interaction sites were within 2 Å of each other, then the move (volume, translation, or rotation) was immediately rejected, or the weight of the trial site (in CBMC molecule exchange or conformational moves)

was set to zero. In addition, a third cutoff based on the COM separation was used to further improve computational efficiency. Consider two molecules A and B each of which has a maximum distance from its COM to any of its own pseudoatoms (d_{COM} (A) and d_{COM} (B)). If the COM of A and B are separated by more than $r_{cut} + d_{COM}(A) + d_{COM}(B)$, then clearly none of their pseudoatoms can lie within r_{cut}, so the individual distances between all these sites need not be computed. A molecule being grown utilizing the CBMC algorithm does not yet have a COM, so the COM truncation is done in a slightly different way. Consider the growth of interaction site *i* on molecule A. The interactions with the sites of molecule B are not computed if the distance from site *i* to the COM of molecule B is greater than $r_{cut} + d_{COM}(B)$. At the start of the simulation, d_{COM} is computed for all molecules and stored in an array. For a given molecule, this distance need only be updated after a successful conformational change (CBMC move or CBMC exchange). For the simulations reported here, the COM-based potential truncation yields a speedup of more than a factor of 2. In general the efficiency of this additional center-of-mass cutoff will increase with decreasing density, increasing ratio between the length of the simulation box and r_{cut}, and increasing number of interaction sites per molecule.

The simulations were carried out for system sizes ranging from 400 molecules for methane to 200 molecules for *n*-dodecane. In addition, a system of 1600 *n*-octane molecules was also simulated and compared to the results for a 200 *n*-octane system in order to assess finite-size effects. The total volume of the two simulation boxes was adjusted so that the liquid phase contained approximately twice as many molecules as the vapor phase. Simulations were equilibrated for at least 5000 MC cycles, during which the chemical potentials, the pressures, and the difference in the number of molecule exchanges were monitored. The production periods consisted of 5000 to 10 000 (OPLS and SKS) or 25 000 (TraPPE) MC cycles. Standard deviations of the ensemble averages were computed by breaking the production runs into five blocks. One thousand MC cycles take approximately 12, 62, and 914 min of CPU time on an Intel Pentium II (at 300 MHz) for systems of 400 ethane, 200 *n*-octane, and 1600 *n*-octane molecules, respectively.

The critical properties are extrapolated from weighted linear fits of the subcritical simulation data to the density scaling law[32] for the critical temperature T_c,

$$\rho_{liq} - \rho_{vap} = B(T - T_c)^{\beta} \quad (6)$$

to the law of rectilinear diameters[33] for the critical density ρ_c,

$$^1/_2(\rho_{liq} + \rho_{vap}) = \rho_c + A(T - T_c) \quad (7)$$

and the Clausius−Clapeyron equation[34] for the critical pressure p_c,

$$\ln p = C + \frac{C'}{T} \quad (8)$$

where ρ_{liq} and ρ_{vap} are the saturated liquid and vapor densities; T and p are the temperature and pressure (obtained from the molecular virial[31]); A, B, C and C' are constants, and β is the critical exponent, which deserves special attention (vide infra). The normal boiling temperature T_b is also estimated from eq 7.

B. Specific Densities and High-Pressure Equation of State. Simulations in the isobaric−isothermal ensemble[35] were used to determine the specific densities of *n*-pentane, *n*-octane, and *n*-dodecane at 298 K and 1 atm. Four types of moves were selected randomly with a fixed probablity of performing a volume move of 0.002, and the remainder equally distributed between CBMC, translation, and rotation. The simulations were carried out for 220 (*n*-pentane), 128 (*n*-octane), and 180 (*n*-dodecane) molecules. Simulations in the canonical ensemble were performed to study the high-pressure *PVT* behavior of *n*-pentane and *n*-decane. The MC moves were equally divided between CBMC, translation, and rotation. The simulations were carried out for 512 *n*-pentane and 256 *n*-decane molecules. The isobaric−isothermal and canonical ensemble simulations consisted of at least 10 000 MC cycles for equilibration and 10 000 MC cycles for production.

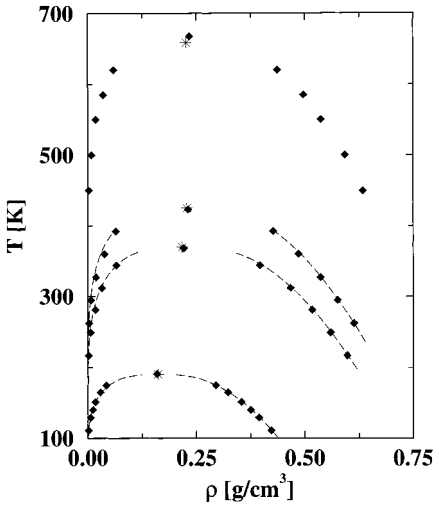

Figure 1. Vapor−liquid coexistence curves for methane, *n*-propane, *n*-butane, and *n*-dodecane. Experimental coexistence data[44] and critical points[45] are shown as long dashed lines and stars. Simulated coexistence densities and extrapolated critical points for the TraPPE force field shown as filled diamonds.

C. Second Virial Coefficients. The second virial coefficient, $B(T)$, of a fully flexible molecule is given by[36,37]

$$B(T) = -2\pi \int [\langle \exp[-U_{inter}(r_{12})/k_B T] \rangle_{\alpha_1,\alpha_2} - 1] r_{12}^2 \, dr_{12} \quad (9)$$

where U_{inter} and r_{12} are the intermolecular interaction energy and the distance between the COM of molecules 1 and 2, and $\langle \cdots \rangle_{\alpha_1,\alpha_2}$ denotes the canonical ensemble average sampled over conformations of molecules 1 and 2, which are Boltzmann weighted solely on their intramolecular energies. We evaluate this average by utilizing two simulation boxes, each containing a single chain which samples conformational space via rotational and CBMC moves. After every 10 Monte Carlo cycles the intermolecular energy for the current two chain conformations is evaluated for COM separations from 0 to 500 Å with a 0.05 Å step size. Once the ensemble average has been computed, the second virial coefficient is determined via numerical integration using the trapezoid rule.[38] The values reported herein were calculated from four separate runs of 10 000 cycles each.

4. Results and Discussion

A. Vapor−Liquid Coexistence Curves. The vapor−liquid coexistence curve (VLCC) (see Figure 1 and Table S1[39]) and the critical properties (see Table 2) calculated for the OPLS methane parameters are in excellent agreement with experiment. Using $\beta = 0.32$, the reduced critical temperature ($T_c^* = T_c/\epsilon$) and number density ($\rho_c^* = \rho_c \sigma^3$) are 1.294 ± 0.009 and 0.311 ± 0.006, respectively. These differ slightly from the earlier

TABLE 2: Normal Boiling Points and Critical Properties Obtained from the Simulations (Using a Critical Exponent $\beta = 0.32$). Subscripts Show the Statistical Uncertainty of the Final Digit. The Experimental Boiling and Critical Points Are Taken from Teja et al.[45]

alkane	force field/expt	T_b [K]	T_c [K]	ρ_c [g/mL]	p_c [MPa]	Z_c
methane	OPLS	111.5_9	191.4_{13}	0.160_3	4.5_{11}	0.28_7
	expt	111.6	190.6	0.162	4.6	0.288
ethane	OPLS	190_1	323_2	0.203_4	5.6_{11}	0.31_6
	SKS	210_2	365_3	0.181_5	6.4_{39}	0.35_{21}
	TraPPE	177_1	304_2	0.206_3	5.1_4	0.30_2
	expt	185	305	0.203	4.9	0.285
propane	TraPPE	222_1	368_2	0.221_3	4.4_1	0.287_8
	expt	231	370	0.217	4.3	0.281
n-butane	TraPPE	261_2	423_4	0.231_6	4.1_4	0.29_3
	expt	273	425	0.228	3.8	0.274
n-pentane	OPLS	327_3	517_5	0.226_7	3.6_{13}	0.27_9
	SKS	326_3	510_4	0.223_6	3.8_9	0.29_7
	TraPPE	296_2	470_2	0.238_4	3.7_1	0.287_9
	expt	309	470	0.230	3.4	0.271
n-octane	OPLS	442_4	656_5	0.235_9	2.8_{23}	0.37_{30}
	SKS	417_1	607_5	0.228_6	3.0_4	0.30_4
	TraPPE 200	388_2	568_3	0.240_5	2.7_3	0.27_3
	TraPPE 1600	386_2	570_2	0.239_2	2.6_1	0.26_1
	expt	399	569	0.232	2.5	0.259
n-dodecane	TraPPE	480_2	667_5	0.235_6	2.3_2	0.30_3
	expt	489	658	0.226	1.8	0.251

simulation results for Lennard-Jonesium reported by Smit and Frenkel[40,41] of $T_c^* = 1.316 \pm 0.006$ and $\rho_c^* = 0.304 \pm 0.006$ for $\beta = 0.32$, but are in better agreement with Panagiotopoulos results[42] for Lennard-Jonesium (using a potential truncation at 5σ) of $T_c^* = 1.281 \pm 0.005$ and $\rho_c^* = 0.32 \pm 0.01$ for $\beta = 1/3$. The differences between Smit's and our results might originate from the fact that we do not include simulation data in the immediate vicinity of the critical temperature in our analysis, as suggested by Panagiotopoulos,[42] whereas Smit used simulation data for $T^* = 1.30$ and 1.31.

The errors reported herein are only the statistical errors, and systematic errors associated with the precise value of β and originating from finite-size effects are not taken into account.[42,43] To illustrate the former uncertainty, we have determined the critical exponent for the *n*-alkanes using the experimental coexistence densities[44] (over a range of temperatures similar to the simulation data) and critical temperatures.[45] The β values range from 0.340 ± 0.002 for methane to 0.307 ± 0.002 for *n*-octane. Using $\beta = 0.34$ to analyze our methane simulation data yields $T^* = 1.311 \pm 0.009$, a value that is 1.3% higher than the the $\beta = 0.32$ result. Using this, we estimate a systematic error due to the uncertainty in β of roughly 1%. From comparison of Panagiotopoulos' GEMC data[42] and Wilding's finite-size scaling study[43] for Lennard-Jonesium, we estimate that the use of finite simulation sizes might also contribute roughly 1% to the systematic error. To investigate finite-size effects in GEMC simulations of chain molecules, we have carried out calculations for 200 and 1600 *n*-octane molecules. Over the entire range of temperatures studied, the results for the two system sizes agree to within their statistical accuracies. The temperature dependence of the density order parameter is shown in Figure 2. For $T \leq 0.95T_c$, there is no evidence of a crossover from nonclassical Ising-like to classical mean-field behavior. The results fall on a straight line for $\beta = 0.32$, while deviations from the straight line are clearly evident for $\beta = 0.5$. However, it should also be noted that the accuracy of the GEMC simulations is not sufficient to determine a more precise value of the scaling exponent. Following from this discussion, it is clear that the LJ well depth for a given pseudoatom cannot be determined from GEMC simulations beyond an accuracy of

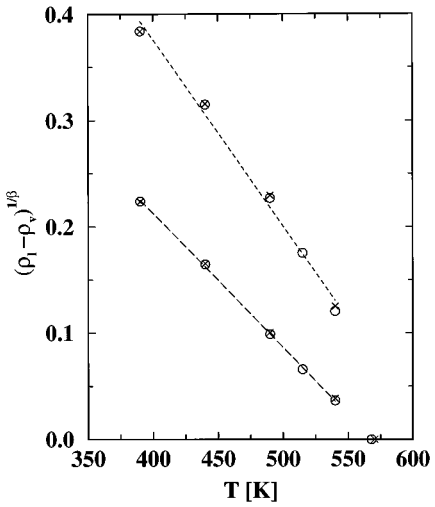

Figure 2. Finite-size effects for *n*-octane using system sizes of 200 (circles) and 1600 (crosses) molecules. Data points and linear regressions for the 200 molecule system size are shown for β values of 0.5 (dotted line) and 0.32 (dashed line). Extrapolated critical points using $\beta = 0.32$ are shown on the *x*-axis.

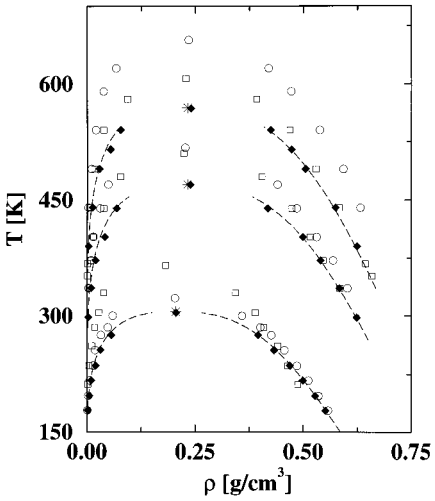

Figure 3. Vapor−liquid coexistence curves for ethane, *n*-pentane, and *n*-octane. Experimental coexistence data[44] and critical points[45] are shown as long dashed lines and stars. Simulation results and extrapolated critical points are shown for OPLS (circles), SKS (squares), and TraPPE (diamonds).

1%. Thus, the OPLS ϵ_{CH_4} value was rounded to 148 K for the TraPPE force field to emphasize the practical limits of fitting this parameter.

The VLCC of ethane was calculated first for the OPLS and SKS force fields (see Figure 3, Tables 2 and S1). The SKS force field, which was designed for the longer alkanes, overestimates T_c by 20% and underestimates ρ_c by 12%. The saturated liquid densities calculated for the SKS force field are too low at low temperatures and too high once the experimental critical point is approached. The OPLS force field performs significantly better for ethane, giving perfect agreement for ρ_c, and a T_c that is only 6% too high. At least for lower temperatures, the OPLS force field predicts accurate liquid densities. It is worth noting that the methyl group LJ parameters of the OPLS force field are different depending on what group the methyl bead is bonded to (see Table 1). It can easily be seen that the OPLS CH_3 parameters for longer alkanes would give less good agreement with the experimental data.

The goal for the fitting of the TraPPE force field parameters was to give agreement with the experimental critical properties,

TABLE 3: Critical Densities, Temperatures, and Root Mean Square Differences between the Simulated and Experimental Liquid Coexistence Densities for the Combinations of σ and ϵ Used To Determine the Final TraPPE Parameters. Statistical Uncertainty of the Final Digit Is Given as a Subscript

ϵ_{CH_3}/k_B [K]	σ_{CH_3} [Å]	ϵ_{CH_2}/k_B [K]	σ_{CH_2} [Å]	T_c [K]	ρ_c [g/mL]	rms [g/mL]
			ethane			
98	3.73	N/A	N/A	304_3	0.205_5	0.0044
98	3.75	N/A	N/A	304_2	0.206_3	0.0026
98	3.77	N/A	N/A	302_3	0.203_5	0.0090
			n-octane			
98	3.75	46	3.95	568_3	0.240_5	0.0044
98	3.75	47	3.91	571_6	0.243_9	0.0117
98	3.75	47	3.93	576_5	0.240_5	0.0152
98	3.75	47	3.95	581_7	0.237_9	0.0112
98	3.75	47	3.97	584_5	0.234_7	0.0161

and coexistence densities to within the statistical accuracy of the simulations. As will be discussed below, this goal appears to be unattainable for the 12−6 Lennard-Jones united-atom model studied. The critical temperature and the saturated liquid densities were chosen as the primary criteria for determining which set of parameters was selected. The TraPPE methyl group parameters were fitted to yield the experimental critical temperature and to minimize the root mean square (rms) deviation between the simulated and experimental saturated liquid densities for ethane. Table 3 shows that the TraPPE simulation results for ethane give a rms deviation from experiment (0.0026 g/mL), which is close to the average standard deviation (0.0027 g/mL) obtained from dividing the simulations into five blocks. For the selected set of Lennard-Jones parameters, the critical temperature and liquid densities are in excellent agreement with experiment (see Figure 3 and Table S1), but ρ_c and p_c are too high, while the boiling point is too low (Table 2). These discrepancies are further discussed at the end of this section.

Following the philosophy that there should be only one set of CH_3 LJ parameters for all *n*-alkanes, the TraPPE methyl parameters were then combined with the SKS methylene parameters and tested for *n*-octane. This hybrid model agreed fairly well with experiment. To search for the optimal set of CH_2 LJ parameters, a systematic variation of the methylene σ from 3.91 to 3.97 Å using $\epsilon/k_B = 47$ K was performed. These results are reported in Table 3. As one would expect, the critical density decreases with increasing σ. However, the critical temperature increases with increasing σ. This at first surprising result is caused by fixing the bond length while increasing σ, i.e., increasing the overlap between pseudoatoms. As has already been demonstrated by Tildesley and co-workers,[45] the critical temperature of a LJ dimer is a function of the ratio between bond length and σ (or the amount of overlap). This complicates the fitting procedure, as a change in σ now requires a corresponding change in ϵ in order to maintain the critical temperature. However, no additional simulations are required since the VLCC can be scaled manually by the ratio of the experimental to simulated critical temperature.[47] The rms deviations for these scaled saturated liquid densities are listed in Table 3. A value of $\sigma = 3.95$ Å for methylene was selected, and the corresponding scaled ϵ/k_B is 46 K. At first it might be surprising that the LJ diameter of a methyl pseudoatom is smaller than that of a methylene group. However, it has to be pointed out that the incremental volume of a methyl group remains much larger than the incremental volume of a methylene group as proposed by Bondi[48] because

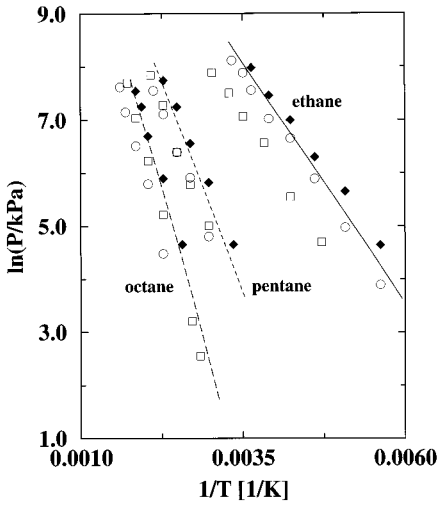

Figure 4. Clausius−Clapeyron plots of the saturated vapor pressure versus the inverse temperature. The experimental data are shown as dashed lines. Circles, squares, and diamonds are used for the simulation data obtained for the OPLS, SKS, and TraPPE force fields, respectively.

of the large overlap between a methylene pseudoatom and its two neighbors. Furthermore, it is plausible that the diameter of a methylene pseudoatom containing two long C−C bonds and two (relatively) short C−H bonds might be larger than that of a pseudoatom containing a single long C−C bond and three short C−H bonds.

The VLCC for ethane, *n*-pentane, and *n*-octane were computed for all three force fields. The results reported here for the OPLS and SKS force fields differ from those reported previously by us.[8,10] The reasons for this are as follows: (i) tail corrections and $r_{cut} = 14$ Å were used here in the simulations for the OPLS force field, while $r_{cut} = 11.5$ Å and no tail corrections were used previously; and (ii) there was an error in the earlier version of our program, which resulted in a systematic underestimation of the tail corrections by a factor of σ^3 for the SKS model.[49] Adding the tail corrections shifts the critical temperatures by approximately 4% when $r_{cut} = 14$ Å($\approx 3.5\sigma$) is used.

Clausius−Clapeyron plots used to determine the critical pressures and the normal boiling points are shown in Figure 4. The critical and normal boiling temperatures, the critical densities, and the critical pressures are depicted as functions of the alkane length for all three force fields in Figures 5−7. The OPLS force field yields good results for the short alkanes, but increasingly overestimates the critical and boiling temperatures as the alkane length increases. The SKS force field predicts too high critical temperatures for all alkanes, but improves as the chain length increases. The TraPPE force field gives a good description of the VLCC and the critical points for the entire range of alkanes.

As should be expected, the trends in T_b and T_c are very similar for the individual force fields. However, the ratio of the simulated to experimental T_b is always lower than the corresponding ratio for T_c (see Figure 5). For the TraPPE force field the T_c^{sim}/T_c^{exp} ratio is close to unity, while the boiling points are consistently underestimated. Since this pattern holds for all three force fields, it appears that this is not caused by the specific set of parameters. The chain-length dependence of ρ_c and p_c are shown in Figures 6 and 7. The TraPPE force field gives too high ρ_c, SKS gives too low ρ_c, and the OPLS values scatter around the experimental values. The theoretical work of Vega and MacDowell[50] predicted that the critical pressure increases to a maximum and then decreases as chain length

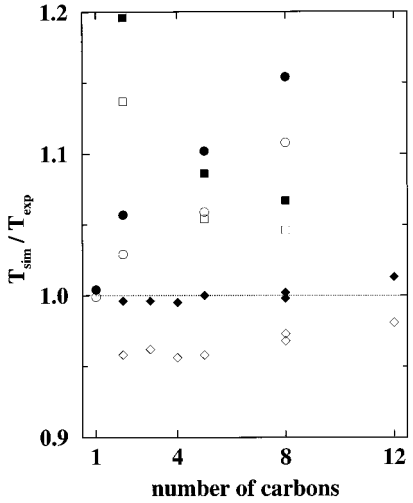

Figure 5. Ratio of simulated to experimental[45] critical temperatures (filled symbols) and normal boiling points (open symbols) versus chain length for the OPLS (circles), SKS (squares), and TraPPE (diamonds) force fields. The two sets of TraPPE results for *n*-octane correspond to the different system sizes (see also Table 2).

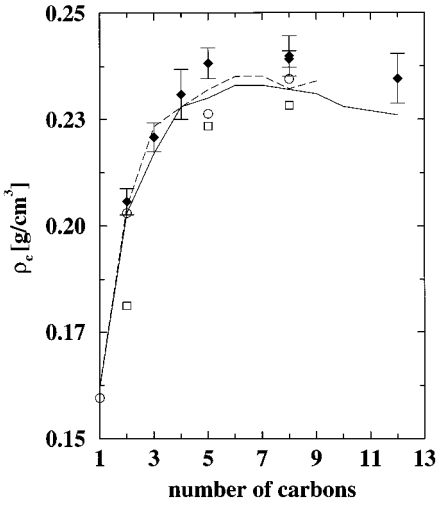

Figure 6. Critical densities versus chain length for the OPLS (circles), SKS (squares), and TraPPE (diamonds) force fields. Experimental data shown from the compilations of ref 44 (dashed line) and ref 45 (solid line). For clarity, error bars are only shown for the TraPPE force field.

increases for any model of linear, overlapping Lennard-Jones spheres. However, the position of this maximum depends on the difference of the interaction energies of methyl and methylene beads. Unfortunately, the large uncertainty associated with determining the critical pressures masks any differences that may exist between the force fields. All three force fields consistently predict too high critical pressures, but capture the general trends in p_c with a maximum around ethane.

While the overall agreement with experiment in VLCC and critical properties obtained for the TraPPE force field is a considerable improvement over the OPLS and SKS force fields, it is clear that also the TraPPE model is not able to reproduce all properties to within the statistical uncertainties. Using the set of constraints listed in the Introduction, a four-parameter united-atom Lennard-Jones model optimized for critical temperatures and saturated liquid densities yields (slightly) too high critical densities and critical pressures and too low boiling points. These all result from having too high vapor densities (or too low heats of vaporization). Puzzling is the fact that no problems are observed for methane. At the moment, we can only speculate about the origin of this deviation. It could be caused

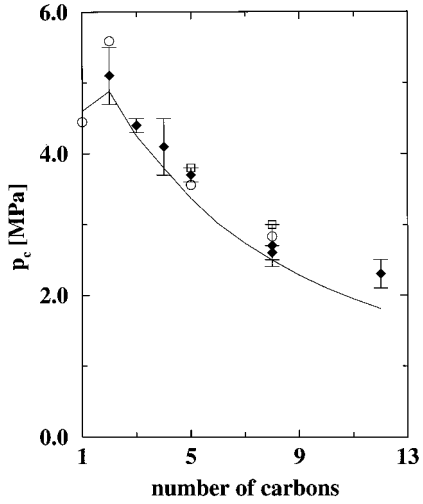

Figure 7. Critical pressures versus chain length for the OPLS (circles), SKS (stars), and TraPPE (diamonds) force fields. Experimental data[45] are shown as a solid line.

TABLE 4: Liquid Densities at Standard Conditions and the Average Root Mean Square Deviation between Simulated and Experimental Saturated Liquid Densities for the TraPPE Force Field

molecule	$\rho_{liq,std}$ (TraPPE) [g/mL]	$\rho_{liq,std}$ (expt) [g/mL]	rms devation [g/mL]
methane	N/A	N/A	0.0018
ethane	N/A	N/A	0.0026
propane	N/A	N/A	0.0035
n-butane	N/A	N/A	0.0026
n-pentane	0.623_2	0.6262	0.0040
n-octane	0.705_3	0.7025	0.0044
n-dodecane	0.754_2	0.7487	N/A

TABLE 5: Pressure versus Temperature Data Computed from Canonical Simulations for "Isochores" of *n*-Pentane and *n*-Decane Using the TraPPE Model. Experimental Pressure versus Temperature Data Are Shown along with the Recommended Corrected Densties.[54,55] Subscripts Show the Statistical Uncertainty of the Final Digit

molecule	T [K]	ρ [g/mL]	p(TraPPE) [MPa]	p(expt) [MPa]
n-pentane	313.15	0.673	60.0_6	60.5
	443.15	0.666	154.2_{11}	160.1
	543.15	0.661	215.5_7	225.3
n-decane	313.15	0.741	21_2	35.7
	453.15	0.733	117_4	153.1
	553.15	0.728	175_3	224.7

by the use of the Lennard-Jones potential function,[51,52] the neglect of explicit three-body interactions, or the united-atom description.[52]

B. Specific Densities and High-Pressure Equation of State. The specific densities at standard conditions for *n*-pentane, *n*-octane, and *n*-dodecane were calculated for the TraPPE model in the isobaric−isothermal ensemble and are listed in Table 4. The calculated liquid densities agree to better than 1% with experiment. Thus for octane and dodecane the TraPPE model yields satisfactory densities at temperatures much lower than those used in the GEMC simulations.

Following Toxvaerd's reports[4,53] on the failure of united-atom models to reproduce the high-pressure equation of state, we have computed liquid pressures for "isochores" of *n*-pentane and *n*-decane using the TraPPE model in the canonical ensemble, as listed in Table 5. To allow for a direct comparison with experimental results, where the volume of the high-pressure vessel changes with T and p, we have performed our simulations

TABLE 6: Comparison of the Second Virial Coefficients for Some *n*-Alkanes. The Experimental Data Are Taken from Dymond and Smith[56] for Ethane and from Smith and Srivastava[44] for the Other Alkanes. The Column SKS* Gives the Results Calculated by Sheng.[60] The Unit for the Second Virial Coefficient is mL/mol. Subscripts Show the Statistical Uncertainty of the Final Digit

alkane	T [K]	expt	OPLS	SKS	SKS*	TraPPE
ethane	298.2	−185	-184_1	-251_2		-159_1
	348.2	−135	-135_1	-188_2		-115_1
	423.2	−88	-89_1	-126_1		-73_1
n-pentane	173	−13005	-5876_{118}	-5787_{184}		-3841_{139}
	247	−2232	-1872_{35}	-1920_{30}		-1407_{14}
	321	−1003	-1012_5	-1024_{34}		-791_{16}
	395	−602	-635_7	-653_{15}		-496_6
n-hexane	207	−9753		-5608_{147}	-2480_{17}	-3838_{80}
	304	−1845		-1718_{29}	-796_4	-1338_{21}
	425	−745		-782_{20}	-396_2	-628_{13}
n-octane	288	−5278	-6029_{195}	-4239_{159}		-3234_{52}
	368	−2179	-2509_{70}	-2061_{18}		-1685_{42}
	448	−1245	-1542_{30}	-1249_{29}		-1018_7
	528	−810	-1027_9	-863_{36}		-676_{31}

at exactly the corrected molar volumes listed in the experimental papers.[54,55] While agreement with experiment for *n*-pentane is acceptable, the results for *n*-decane are obviously too low. It is unclear which approximation used in the TraPPE model causes these deviations.

C. Second Virial Coefficients and Compressibility Factors. The calculation of second virial coefficients reveals some of the limitations inherent to the relatively simple alkane models used here. While the TraPPE LJ parameters give a more accurate VLCC for ethane, they do not reproduce the experimental[56] second virial coefficients as well as the OPLS force field (see Table 6). The TraPPE force field consistently underestimates the magnitude of the second virial coefficient for all alkanes over the entire range of temperatures. The main reason for this disagreement is that the TraPPE force field has been parametrized to reproduce the VLCC and, in particular, the saturated liquid densities using simple LJ pair potentials, that is, the specific sets of ϵ and σ values yield *effective* pair potentials and not the *true* pair potentials. These effective pair potentials implicitly include many-body effects. For nonpolar species the dominant many-body term is the Axilrod−Teller triple dipole term,[57] which is repulsive in nature, can be accounted for with a potential of the r^{-6} form,[58] and is often found to be approximately 10% of the leading two-body term.[31] Thus by design a good effective pair potential should underestimate the magnitude of the second virial coefficient, since U_{inter} in eq 9 is not the true pair potential. The use of effective pair potentials might be sufficient to rationalize the differences (10−20%) between experimental data and the TraPPE force field at the higher temperatures. However, the much larger disagreement at the lower temperatures (e.g., pentane at 173 K and hexane at 207 K) cannot be explained solely by the difference between effective and true pair potentials. We can only speculate that at these low temperatures, which are close to the melting temperatures, the united-atom description might not be sufficient in detail to account for the structures of the alkanes. It remains to be seen whether all-atom models will perform better in this respect. Here it should be noted that a recent united-atom LJ alkane model that uses four different pseudoatoms (eight LJ parameters)[59] yields better results for the second virial coefficients of the shorter alkanes.

The second virial coefficients calculated for the OPLS and SKS force fields are more difficult to compare to their experimental counterparts because differences arising from the use of effective pair potentials compete with the fact that both force fields are overbound, i.e., yield too high T_c. For example, the OPLS force field underestimates the magnitude of the second virial coefficient for pentane at 247 K and overestimates it at 395 K, while the values for octane are too large over the entire range of temperatures.

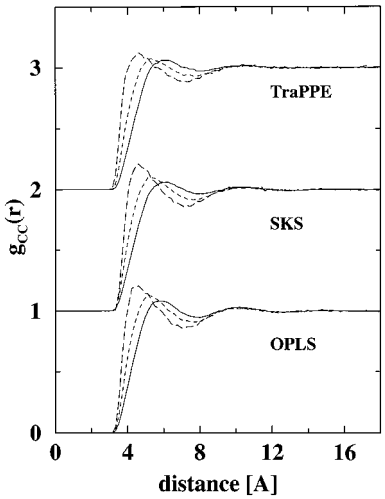

Figure 8. Intermolecular site−site radial distribution functions for the liquid phase of *n*-octane at 490 K. For clarity, curves are vertically displaced by one unit. The three curves for each force field are methyl−methyl (long dashed), methyl−methylene (short dashed), and methylene−methylene (solid).

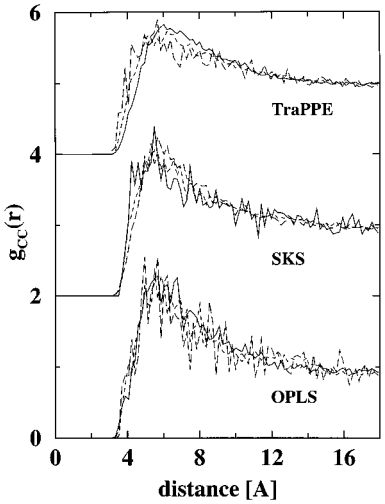

Figure 9. Intermolecular site−site radial distribution functions for the vapor phase of *n*-octane at 490 K. Line styles as in Figure 8.

Sheng[60] has previously calculated the second virial coefficient for hexane using the SKS force field, and the results are also listed in Table 6. The large disagreement of roughly a factor of 2 between Sheng's data and our calculations is very puzzling, but cannot be resolved here. In Sheng's method, the two molecules are both placed in a single box and allowed to sample phase space with the acceptance rate of the Monte Carlo moves based solely on intramolecular interactions. The Mayer function (eq 9) is then evaluated periodically.[60]

The compressibilty factors were computed for each temperature and at the critical point, as listed in Table S1 and Table 2. The TraPPE results generally agree with experiment to within the error bars, but overall are slightly too high. The critical compressibilities are not precise enough to determine whether they follow the experimentally observed trend of decreasing with increasing chain length.

TABLE 7: Fraction of Gauche Defects, f_g, and Mean Square End-to-End Length, R_e^2 in Units of Å^2, in the Liquid and Vapor Phases for *n*-Octane and *n*-Dodecane Using the TraPPE Force Field. Subscripts Show the Statistical Uncertainty of the Final Digit

alkane	temp (K)	f_g(liq)	f_g(vap)	R_e^2(liq)	R_e^2(vap)
n-octane	390	0.331	0.345	59.27_7	58.34_{11}
$N = 200$	440	0.355	0.370	57.96_8	57.22_5
	490	0.373	0.383	56.81_6	56.27_9
	515	0.382	0.389	56.35_{13}	55.96_9
	540	0.387	0.395	55.94_7	55.59_8
n-dodecane	450	0.349	0.370	121.1_2	115.7_5
	500	0.370	0.379	117.7_7	113.4_4
	550	0.384	0.391	114.7_2	111.5_2
	585	0.395	0.402	113.1_3	110.4_3
	620	0.404	0.413	111.4_3	109.5_2

D. Radial Distribution Functions. Site−site radial distribution functions (RDFs) were calculated for all simulations. As a typical example, the RDFs of *n*-octane at 490 K are shown for the three force fields in Figures 8 and 9. The most striking observation is the similarity of the RDFs. At this temperature the saturated liquid densities of octane are 0.592, 0.529, and 0.505 g/mL for the OPLS, SKS, and TraPPE force fields (the corresponding experimental value is 0.510 g/mL). However, a change of 15% in the density seems to have little effect on the RDF. For all three force fields the methyl−methyl peak is stronger and occurs at a shorter separation than the methyl−methylene and methylene−methylene peaks in the liquid phase. The methyl−methyl peak position is essentially the same for all three force fields, demonstrating that the RDF is not a good criterion to decide whether or not the same LJ diameter should be used for both methyl and methylene pseudoatoms. In the vapor phases only one peak is observed for all RDFs. At first it might be surprising that the peak heights of these vapor-phase RDFs are larger than those of the corresponding liquid-phase RDFs. However, this supposedly enhanced structure in the vapor phase should always be viewed in the context of the much lower density. For example, for the TraPPE force field the numbers of nearest neighbors obtained from the integrals of the methyl−methyl RDFs (truncated at 15 and 7.5 Å for the vapor and liquid phase, respectively) are 0.4 and 4.2 pseudoatoms for the vapor and liquid phase. The vapor-phase peaks for the OPLS and SKS force fields are stronger, because these force fields have higher T_c. When the vapor-phase RDFs are compared for the same reduced temperature, the differences in peak heights largely disappear.

E. Chain Conformations. The conformational statistics are very similar for all three force fields studied here. This is no surprise since the same dihedral potential (eq 5) was employed for all three force fields. For all flexible alkanes (containing at least one dihedral angle) the number of gauche defects increases and the mean square end-to-end length decreases in regular fashion with increasing temperature. For the shorter alkanes (butane and pentane) and for a given force field and a given temperature, the fractions of dihedral angles in the gauche state and the mean square end-to-end lengths are identical between vapor and liquid phase (to within the statistical uncertainties). In contrast, for the longer alkanes (octane and dodecane) some differences in conformational statistics appear between the two phase (see Table 7). The fractions of gauche angles are consistently higher in the vapor phase than in the liquid phase, and correspondingly the mean square end-to-end lengths are lower in the vapor phase for *n*-octane and *n*-dodecane. These admittedly very small differences are an indication that in the absence of neighboring molecules the longer chains prefer to coil onto themselves due to the nonbonded interactions between distant pseudoatoms.

TABLE 8: Normalized Distribution of Gauche Defects for *n*-Octane and *n*-Dodecane Averaged over the Five Temperatures Given in Table 4. Torsional Angles Are Listed by the Atoms That Make Up the Central Bond. Bonds That Are Identical Due to Symmetry Are Shown with the Same Letter Superscript. Subscripts Show the Statistical Uncertainty of the Final Digit

alkane	bond	P_g(liq)	P_g(vap)
n-octane	$2-3^a$	1.09_2	1.10_1
	$3-4^b$	0.93_2	0.93_2
	4−5	0.97_1	0.96_1
	$5-6^b$	0.91_1	0.92_1
	$6-7^a$	1.10_1	1.09_1
n-dodecane	$2-3^z$	1.12_1	1.13_2
	$3-4^y$	0.94_1	0.92_2
	$4-5^x$	0.98_1	0.99_3
	$5-6^w$	0.97_1	0.99_2
	6−7	0.97_1	0.99_2
	$7-8^w$	0.98_1	0.98_2
	$8-9^x$	0.98_1	0.97_1
	$9-10^y$	0.94_1	0.92_2
	$10-11^z$	1.12_2	1.12_2

The distribution of gauche defects along the chains has also been analyzed, and an interesting pattern is observed (see Table 8). While the dihedral angles at the end of the molecules are most likely to show a gauche defect, the probability to find a defect is lowest for the bonds adjacent to the end dihedrals. The central bonds have an average propensity for gauche defects. The symmetry of the distributions of gauche defects is a very good indication that the conformational degrees of freedom are sampled very well with the configurational-bias Monte Carlo algorithm.

5. Concluding Remarks

Configurational-bias Monte Carlo calculations in the Gibbs ensemble were used to determine the vapor−liquid coexistence curves of linear alkanes for three different united-atom force fields. The OPLS force field[7] gives reasonable results for short alkanes, but overpredicts the critical temperatures of longer alkanes. The SKS force field[9,10] gives too high critical temperatures for the shorter alkanes, but approaches the experimental data as the chain length increases. The OPLS methane parameters and new methyl and methylene parameters were combined into the transferable potentials for phase equilibria (TraPPE) force field. The TraPPE force field accurately describes the vapor−liquid coexistence curves and critical properties of linear alkanes from methane to dodecane using a single set of parameters for each pseudoatom. Small but systematic deviations from experiment are observed for the vapor densities and pressures. None of the three force fields are able to reproduce experimental second virial coefficients, which is mainly due to the use of effective pair potentials. Conversely, it is expected that a pair-potential-based force field parameterized to reproduce the second virial coefficients will fail to describe the vapor−liquid coexistence curves. Radial distribution functions vary to a surprisingly small extent between the three force fields. The first methyl−methyl peaks are stronger and at closer separations than the first methylene−methylene peak, even for force fields with identical Lennard-Jones diameters for methyl and methylene pseudoatoms. The longer alkanes seem to prefer more coily conformations in the vapor phase than in the liquid phase, which is evident from shorter mean square end-to-end lengths and larger fractions of gauche defects.

Acknowledgment. We would like to acknowledge many stimulating discussions with Peter Cummings, Juan de Pablo, and Thanasis Panagiotopoulos and the thoughtful comments of the two reviewers. Financial support from the Petroleum Research Fund, administered by the American Chemical Society (Grant No. 29960-AC9), through a Camille and Henry Dreyfus New Faculty Award, and through a McKnight Fellowship is gratefully acknowledged. M.G.M. would like to thank the Graduate School, University of Minnesota, for the award of a Graduate School Fellowship, and the Department of Energy for a Computational Science Graduate Fellowship. Part of the computer resources were provided by the Minnesota Supercomputer Institute through the University of Minnesota−IBM Shared Research Project and NSF Grant CDA-9502979.

Supporting Information Available: See ref 39 (3 pages). Ordering information is given on any current masthead page.

References and Notes

(1) Williams, D. E. *J. Chem. Phys*. **1967**, *47*, 4680.
(2) Ryckaert, J. P.; Bellemans, A. *Faraday Discuss. Chem. Soc*. **1978**, *66*, 95.
(3) Rodger, P. M.; Stone, A. J.; Tildesley, D. J. *Molec. Simul*. **1992**, *8*, 145.
(4) Toxvaerd, S. *J. Chem. Phys*. **1990**, *93*, 4290.
(5) Lago, S.; Garzon, B.; Calero, S.; Vega, C. *J. Phys. Chem. B* **1997**, *101*, 6763.
(6) Paul, W.; Yoon, D.Y.; Smith, G. D. *J. Chem. Phys*. **1995**, *103*, 1702.
(7) Jorgensen, W. L.; Madura, J. D.; Swenson, C. J. *J. Am. Chem. Soc*. **1984**, *106*, 813.
(8) Siepmann, J. I.; Karaborni, S.; Smit, B. *J. Am. Chem. Soc*. **1993**, *115*, 6454.
(9) Siepmann, J. I.; Karaborni, S.; Smit, B. *Nature* **1993**, *365*, 330.
(10) Smit, B.; Karaborni, S.; Siepmann, J. I. *J. Chem. Phys*. **1995**, *102*, 2126.
(11) Martin, M. G.; Siepmann, J. I. *J. Am. Chem. Soc*. **1997**, *119*, 8921. In these calculations a preliminary version of the TraPPE methyl group parameters ($\sigma = 3.77$ Å, $\epsilon/k_B = 98.1$ K) was used in combination with the SKS methylene group parameters.
(12) Martin, M. G.; Siepmann, J. I. In preparation.
(13) Lorentz, H. A. *Ann. Phys*. **1881**, *12*, 127.
(14) Berthelot, D. C. *R. Hebd. Séanc. Acad. Sci., Paris* **1898**, *126*, 1703.
(15) Van der Ploeg, P.; Berendsen, H. J. C. *J. Chem. Phys*. **1982**, *94*, 3271.
(16) Mooij, G. C. A. M.; Frenkel, D.; Smit, B. *J. Phys.: Condens. Matter* **1992**, *4*, L255.
(17) Laso, M; de Pablo, J. J.; Suter, U. W. *J. Chem. Phys*. **1992**, *97*, 2817.
(18) Panagiotopoulos, A. Z. *Mol. Phys*. **1987**, *61*, 813.
(19) Panagiotopoulos, A. Z.; Quirke, N.; Stapleton, M.; Tildesley, D. J. *Mol. Phys*. **1988**, *63*, 527.
(20) Smit, B.; de Smedt, P.; Frenkel, D. *Mol. Phys*. **1989**, *68*, 931.
(21) Siepmann, J. I. *Mol. Phys*. **1990**, *70*, 1145.
(22) Siepmann, J. I.; Frenkel, D. *Mol. Phys*. **1992**, *75*, 59.
(23) Frenkel, D.; Mooij, G. C. A. M.; Smit, B. *J. Phys.: Condens. Matter* **1992**, *4*, 3053.
(24) de Pablo, J. J.; Laso, M.; Suter, U. W. *J. Chem. Phys*. **1992**, *96*, 2395.
(25) Barker, J. A.; Watts, R. O. *Chem. Phys. Lett*. **1969**, *3*, 144.
(26) Siepmann, J. I.; McDonald, I. R. *Mol. Phys*. **1993**, *79*, 457.
(27) Spyriouni, T.; Economou, I. G.; Theodorou, D. N. *Macromolecules* **1997**, *30*, 4755.
(28) Vlugt, T. J. H.; Martin, M. G.; Smit, B.; Siepmann, J. I.; Krishna, R. *Mol. Phys*., in press.
(29) Esselink, K.; Loyens, L. D. J. C.; Smit, B. *Phys. Rev. E* **1995**, *51*, 1560.
(30) Mackie, A. D.; Tavitian, B.; Boutin, A.; Fuchs, A. H. *Mol. Simul*. **1997**, *19*, 1.
(31) Allen, M. P.; Tildesley, D. J.; *Computer Simulation of Liquids*; Oxford University Press: Oxford, 1987.
(32) Rowlinson, J. S.; Widom, B. *Molecular Theory of Capillarity*; Oxford University Press: New York, 1989; p 261.
(33) Rowlinson, J. S., Swinton, F. L. *Liquids and Liquid Mixtures*, 3rd ed.; Butterworth: London, 1982; pp 70−75.
(34) Atkins, P. W. *Physical Chemistry*, 4th ed.; W.H. Freeman and Company: New York, 1990; Chapter 6.
(35) McDonald, I. R. *Mol. Phys*. **1972**, *23*, 41.
(36) McQuarrie, D. A. *Statistical Mechanics*; Harper and Row: New York, 1976; Chapter 12.
(37) Harismiadis, V. I.; Szleifer, I. *Mol. Phys*. **1994**, *81*, 851.
(38) Cheney, W.; Kincaid, D. *Numerical Mathematics and Computing*, 3rd ed.; Brooks/Cole: Pacific Grove, 1994; Chapter 5.
(39) The numerical values of the saturated vapor pressures, mean square end-to-end lengths, and coexistence densities for all simulations are listed in the Supporting Information (Table S1).
(40) Smit, B. Ph.D. Dissertation, Rijksuniversiteit te Utrecht, 1990.
(41) Smit, B. *J. Chem. Phys*. **1992**, *96*, 8639.
(42) Panagiotopoulos, A. Z. *Int. J. Thermophys*. **1994**, *15*, 1057.
(43) Wilding, N. B. *Phys. Rev. E* **1995**, *52*, 602.
(44) Smith, B. D.; Srivastava, R. *Thermodynamic Data for Pure Compounds: Part A Hydrocarbons and Ketones*; Elsevier: Amsterdam, 1986.
(45) Teja, A. S.; Lee, R. J.; Rosenthal, D.; Anselme, M. *Fluid Phase Equilib*. **1990**, *56*, 153.
(46) Galassi, G.; Tildesley, D. J. *Mol. Simul*. **1994**, *13*, 11.
(47) This is only an approximate procedure since different ϵ values are used for methyl and methylene segments and the value of the former has already been set from the calculations for ethane.
(48) Bondi, A. *J. Phys. Chem*. **1964**, *68*, 441.
(49) Siepmann, J. I.; Martin, M. G.; Mundy, C. J.; Klein, M. L. *Mol. Phys.* **1997**, *90*, 687.
(50) Vega, C.; MacDowell, L. G. *Mol. Phys*. **1996**, *88*, 1575.
(51) Panagiotopoulos, A. Z. Personal communication.
(52) Chen, B.; Martin, M. G.; Siepmann, J. I. *J. Phys. Chem*. **1998**, *102*, 2578.
(53) Toxvaerd, S. *J. Chem. Phys*. **1997**, *107*, 5197.
(54) Gehrig, M.; Lentz, H. *J. Chem. Thermodyn*. **1979**, *11*, 291.
(55) Gehrig, M.; Lentz, H. *J. Chem. Thermodyn*. **1983**, *15*, 1159.
(56) Dymond, J. H.; Smith, E. B. *The Virial Coefficients of Pure Gasses and Mixtures: A Critical Compilation*; Clarendon Press: Oxford, 1980.
(57) Axilrod, B. M.; Teller, E. *J. Chem. Phys*. **1943**, *11*, 299.
(58) Stenschke, H. *J. Chem. Phys*. **1994**, *100*, 4705.
(59) Nath, S. K.; Escobedo, F. A.; de Pablo, J. J. *J. Chem. Phys*., submitted for publication.
(60) Sheng, Y.-J. Ph.D. Dissertation, Cornell University, 1995.